Title
Extracting kinetic information from human motor cortical signals

Authors
Flint, Robert D
Wang, Po T
Wright, Zachary A
et al.

Publication Date
2014-11-01

DOI
10.1016/j.neuroimage.2014.07.049

Peer reviewed

NeuroImage 101 (2014) 695–703

Contents lists available at ScienceDirect

NeuroImage

journal homepage: www.elsevier.com/locate/ynimg

Extracting kinetic information from human motor cortical signals

Robert D. Flint [a,*], Po T. Wang [b], Zachary A. Wright [a], Christine E. King [b], Max O. Krucoff [c], Stephan U. Schuele [a], Joshua M. Rosenow [d], Frank P.K. Hsu [e], Charles Y. Liu [f,g], Jack J. Lin [h], Mona Sazgar [h], David E. Millett [i,j], Susan J. Shaw [i,j], Zoran Nenadic [b,k], An H. Do [h], Marc W. Slutzky [a,l,m,n]

[a] Department of Neurology, Northwestern University, Chicago, IL 60611, USA
[b] Department of Biomedical Engineering, University of California, Irvine, Irvine, CA 92617, USA
[c] Division of Neurosurgery, Duke University, Durham, NC, USA
[d] Department of Neurosurgery, Northwestern University, Chicago, IL 60611, USA
[e] Department of Neurosurgery, University of California, Irvine, Irvine, CA 92617, USA
[f] Department of Neurosurgery, Rancho Los Amigos National Rehabilitation Center, Downey, CA 90242, USA
[g] Department of Neurosurgery, University of Southern California, Los Angeles, CA 90033, USA
[h] Department of Neurology, University of California, Irvine, Irvine, CA 92617, USA
[i] Department of Neurology, Rancho Los Amigos National Rehabilitation Center, Downey, CA 90242, USA
[j] Department of Neurology, University of Southern California, Los Angeles, CA 90033, USA
[k] Department of Electrical Engineering and Computer Science, University of California, Irvine, Irvine, CA 92617, USA
[l] Department of Physiology, Northwestern University, Chicago, IL 60611, USA
[m] Department of Physical Medicine & Rehabilitation, Northwestern University, Chicago, IL 60611, USA
[n] The Rehabilitation Institute of Chicago, Chicago, IL 60611, USA

ARTICLE INFO

Article history:
Accepted 22 July 2014
Available online 2 August 2014

Keywords:
Electrocorticography
Force
Decoding
EMG
Brain–machine interface
Motor cortex

ABSTRACT

Brain machine interfaces (BMIs) have the potential to provide intuitive control of neuroprostheses to restore grasp to patients with paralyzed or amputated upper limbs. For these neuroprostheses to function, the ability to accurately control grasp force is critical. Grasp force can be decoded from neuronal spikes in monkeys, and hand kinematics can be decoded using electrocorticogram (ECoG) signals recorded from the surface of the human motor cortex. We hypothesized that kinetic information about grasping could also be extracted from ECoG, and sought to decode continuously-graded grasp force. In this study, we decoded isometric pinch force with high accuracy from ECoG in 10 human subjects. The predicted signals explained from 22% to 88% (60 ± 6%, mean ± SE) of the variance in the actual force generated. We also decoded muscle activity in the finger flexors, with similar accuracy to force decoding. We found that high gamma band and time domain features of the ECoG signal were most informative about kinetics, similar to our previous findings with intracortical LFPs. In addition, we found that peak cortical representations of force applied by the index and little fingers were separated by only about 4 mm. Thus, ECoG can be used to decode not only kinematics, but also kinetics of movement. This is an important step toward restoring intuitively-controlled grasp to impaired patients.

Introduction

The ability to grasp is critical in daily life, but the neural control of grasping is still not fully understood (Castiello and Begliomini, 2008; Davare et al., 2011). Better knowledge of grasp encoding in the brain could lead to restoration of grasp to people who have lost it because of amputation or paralysis from spinal cord injury, stroke, or amyotrophic lateral sclerosis. Brain machine interfaces (BMIs) use directly-decoded brain signals to control an external device such as a computer cursor (Hochberg et al., 2006; W. Wang et al., 2013), prosthetic arm or hand (Collinger et al., 2013; Fifer et al., 2014; Hochberg et al., 2012; Yanagisawa et al., 2011), or functional electrical stimulation (FES) of paralyzed muscles (Ethier et al., 2012; Moritz et al., 2008). In particular, restoring movement to a paralyzed hand via FES has the potential to grant intuitive control over grasp, which could greatly improve the quality of life for patients with spinal cord injury or stroke (Andersen et al., 2004).

Most existing BMI studies involving grasp have concentrated on decoding kinematics from cortical signals. However, grasping involves a combination of kinematic and kinetic factors (Danion et al., 2013; Krakauer et al., 1999). While a hand neuroprosthesis could be controlled by a BMI that classifies discrete hand grasps or continuous finger movements, fine control of grasp force is essential for accurate manipulation of objects. Thus, for patients to safely and successfully interact with their environment, BMIs will need to enable continuous and accurate control of grasp force by the neuroprosthesis.

* Corresponding author at: 303 E. Superior Ave., Lurie 8-231, Chicago, IL 60611, USA.
E-mail address: r-flint@northwestern.edu (R.D. Flint).

http://dx.doi.org/10.1016/j.neuroimage.2014.07.049
1053-8119/

In monkeys, hand shape (Spinks et al., 2008) and individual finger movement (Aggarwal et al., 2008) can be decoded discretely from neuronal action potentials (spikes), local field potentials (LFPs), or cortical surface potentials (electrocorticography, ECoG; see Chestek et al., 2013; Kubanek et al., 2009) in the primary motor cortex (M1). In addition, spikes in the premotor cortex modulate with grasp type (Townsend et al., 2011). Continuous finger joint positions can also be decoded using spikes (Aggarwal et al., 2013; Ben Hamed et al., 2007; Vargas-Irwin et al., 2010), LFPs (Zhuang et al., 2010), and ECoG (Acharya et al., 2010; Miller et al., 2009). Spike-based BMIs have been used to control continuous grasp aperture (Collinger et al., 2013; Hochberg et al., 2012). An ECoG-based BMI has been used by a few subjects to move a prosthetic hand to one of two discretely-decoded hand postures, but not manipulate objects (Yanagisawa et al., 2011).

To manipulate objects, control of grasp kinetics (force and muscle activation) is critical. However, less is known about the cortical control of grasp kinetics than about the control of kinematics. Spikes have been shown to correlate with grasp force in M1 (Boudreau et al., 2001; Carmena et al., 2003; Evarts et al., 1983; Hendrix et al., 2009), and a spike-based BMI has been used to control grip force in monkeys (Carmena et al., 2003). The representation of force in the dorsal premotor cortex is not as clear, with some finding modulation of spikes with grasp force (Hepp-Reymond et al., 1999), while others did not (Boudreau et al., 2001). Using ECoG from motor and premotor cortices, a study requiring subjects to lift objects with two different weights showed little effect of weight on grasp type decoding, and modest ability to decode the discrete weights (Pistohl et al., 2012). It is unclear if the inconsistencies among studies reflect a complex relationship between force and neural activity, or if the spatial distribution of the brain's force representation has not yet been accurately specified.

Ideally, a neuroprosthetic hand would continuously modulate the force it applies by decoding the user's intended grasp force continuously. Alternatively, FES could be used to activate paralyzed muscles. Studies in monkeys have shown that BMIs could restore movement to a paralyzed hand by using decoded muscle activity from M1 spikes to drive FES (Ethier et al., 2012; Moritz et al., 2008; Pohlmeyer et al., 2009). These arm and finger muscle activations can also be decoded using intracortical M1 LFPs in monkeys (Flint et al., 2012a). Here, we use ECoG to decode the continuous grasp force and finger muscle activity produced by 10 human subjects while they perform an isometric grasp task. In 3 subjects, we decoded force and muscle activity using microwire-ECoG data.

Methods

Subjects and surgical implantation

This study included 10 human participants (4 females, 6 males, ages 20–49, referred to in chronological order as S1, S2,…S10) who were undergoing intracranial monitoring prior to surgery for treatment of medication-refractory epilepsy. All experiments for S1–S4 were performed under protocols approved by the institutional review board of Northwestern University (S1 through S4, protocol #00013311). Experiments for S5–S10 were performed at the University of California at Irvine (IRB protocol #2009-7114) or Rancho Los Amigos National Rehabilitation Center (study #BCI-11-02). All subjects gave written informed consent to participate in the study. Electrode placement was determined by clinical need. Subjects were recruited for the study if their monitoring arrays were expected to cover the hand area of the primary motor cortex. During surgery, arrays were placed in reference to anatomical landmarks, using intraoperative stealth MRI co-registration. In 7 patients (S1, S3–S7, S9), we used standard clinical arrays with 2.3 mm exposed area, 10 mm interelectrode spacing (PMT, Inc. for S1, S3 and S4, and Integra, Inc., for S5–S7 and S9). We implanted subjects S8 and S10 with 8 × 8 "medium-density" ECoG arrays, with 1.5 mm disks spaced 4 mm apart (Integra). In 3 subjects (S2–S4), we implanted surface microwire arrays, with 75 μm diameter and 1 mm interelectrode spacing (16 channel arrays in a diamond configuration, PMT, S2–S4). Post-operative array locations were confirmed using co-registration of pre- or post-operative 1.5 T MRI and post-operative CT images. We performed cortical surface reconstruction and electrode colocalization using either a modification of the techniques presented in Hermes et al. (2010), or according to the method of P.T. Wang et al. (2013). Subjects S8 and S10 could not have MRIs due to metal in the body, so we localized the electrodes from X-rays using the technique of Miller et al. (2007).

Experimental protocol

During each experimental session, subjects were instructed to squeeze a force sensor between their thumb and index finger in a precision grasp. Subjects S8, S9, and S10 also squeezed with their thumb and fifth (or "little") finger in separate experiments. We recorded the isometric force produced simultaneously with ECoG (see Signal acquisition section). The isometric force behavior was performed with the hand contralateral to the recording array. We used a custom-built force sensor based on a 1 DOF load cell (Futek LRF350). Force signals were amplified with a gain of 10,000 (Honeywell model UV in-line amplifier) before being digitized. Beginning with S2, we gave subjects at Northwestern continuous visual feedback of applied force via a computer cursor, and instructed them to perform a 1D random force target-pursuit task. During this task, the subjects attempted to acquire and hold the cursor in each force target for 0.1 s. Feedback was provided using a customized module in BCI2000 (Schalk et al., 2004). Data from subjects S5–S10 was recorded at the University of California at Irvine (UCI), or at Rancho Los Amigos National Rehabilitation Center. Our acquisition hardware at those locations did not allow us to utilize the visual feedback software, so S5–S10 performed self-paced squeezes of self-determined, varying force levels.

Signal acquisition

For subject S1, ECoG signals were digitized at 500 Hz (Nihon Kohden EEG-1100) and force signals were sampled at 500 Hz using a TDT RZ2 Bioamp (Tucker Davis Technologies). The Nihon Kohden and TDT data were synchronized using a TTL pulse prior to analysis. For subjects S2, S3, and S4, both ECoG and force were analog high-pass filtered at 1 Hz and sampled at 1 kHz using the TDT Bioamp and BCI2000 software. For S5–S10, ECoG was sampled at 2048 Hz using 2 linked NeXus-32B amplifiers (20× pre-amp gain, linear phase digital low-pass filtered at 553 Hz; Mind Media). ECoG was common average referenced by the NeXus amplifier before digitization. Force signals for S5–S10 were digitized at 4 kHz with a Biopac MP150 (1000× pre-amp gain), interfaced with custom MATLAB software. The ECoG and force data acquisition devices were synchronized via TTL pulse. Both ECoG and force data were downsampled to 1 kHz in S5–S10 and digitally high-pass filtered at 0.1 Hz (2nd order Butterworth FIR, forward and backward) prior to further analysis.

In S2–S5, S7, S9, and S10 we recorded electromyograms (EMGs) from extrinsic finger flexors (flexor digitorum superficialis). EMGs for S2, S3, and S4 were acquired with surface electrodes (Delsys Bagnoli-8), pre-amplified with gain of 1000 and then digitized using the TDT system. For S5, S7, S9, and S10 EMGs were digitized with a Biopac MP150 EMG amplifier.

Decoding continuous kinetics

We decoded force from ECoG using techniques similar to those we have previously used to decode movement kinematics (Flint et al., 2012b) and muscle activation (Flint et al., 2012a) from intracranial spikes and LFPs. Briefly, we divided each channel of ECoG into its smoothed time-domain representation, the local motor potential

(LMP, Mehring et al., 2004; Schalk et al., 2007), and its frequency or spectral representation. We calculated spectral power in 5 bands using the discrete Fourier transform: 0–4 Hz, 7–20 Hz, 70–115 Hz, 130–200 Hz, and 200–300 Hz (power line frequency was 60 Hz). The 0–4 Hz band actually started at 0.1 Hz in S5–S10 and 1 Hz in S1–S4; we use 0–4 Hz as a label for brevity. For subject S1, we did not use the power in the 200–300 Hz band, due to the 500 Hz sampling rate. Together, the LMP and spectral power bands comprised 6 features per channel (except for S1). We ranked the features from all electrodes by the absolute value of their correlation coefficient with the force signal, and selected the top 90% of features. Feature selection was performed on training data, not test data (see below for details on the cross-validation). We decoded grasp force and EMG with these features using a Wiener cascade filter, which adjusts the output of a standard linear multi-input, single-output filter (i.e. Wiener filter) by convolving it with a static nonlinearity (Hunter and Korenberg, 1986; Westwick et al., 2006). In this case, the nonlinearity was a 3rd order polynomial. We employed a ridge regression technique to reduce the likelihood of overfitting (Fagg et al., 2009). Following Suminski et al. (2010), the Wiener filter can be expressed as

$$F(t) = \sum_{j=-10}^{0} \sum_{i=1}^{N_{feat}} a_{ij} f(i, t+j), \quad (1)$$

where $F(t)$ is the force signal, $f(i, j)$ represents the value of feature i at time lag j, a_{ij} is the filter coefficient for that time lag, N_{feat} is the number of features, and t is the current time. As indicated in the equation, we included a time history of 10 lags into the past. The formulation of the ridge regression specifies a solution for the coefficients

$$a = \left(f^T f + \lambda I\right)^{-1} f^T F, \quad (2)$$

where λ is a regularization constant and I is the identity matrix.

We measured the accuracy of our decoding by calculating the fraction of variance accounted for (FVAF) between predicted and actual force signals. The FVAF is a more stringent measure of the covariation between predicted and actual signals, compared with the coefficient of determination (r^2, see Fagg et al., 2009). The FVAF has a range of [−∞, 1]. We calculated the FVAF using 11-fold cross-validation. To obtain the FVAF for each fold, we used 9 of the 10 folds to train the Wiener cascade decoder. The 10th non-test fold was used for parameter validation, allowing us to optimize the λ parameter for each subject without introducing bias (Fagg et al., 2009). The 11th fold was used to test the decoder performance. We selected values for the other parameters, such as the Fourier window length (256 points), bin size (0.1 s), and bin overlap (156 points), consistent with previous offline and online decoding of movement (Flint et al., 2012b, 2013).

To decode EMG activity, we calculated the envelope of the EMG signal prior to building the linear decoder. We high pass filtered (2nd order Butterworth FIR) the EMG at 50 Hz rectified the signal, then low-pass filtered at 5 Hz to obtain the EMG envelope for prediction. All filtering was performed both forward and backward to avoid delays in the predicted output. This was the same approach we have used previously (Flint et al., 2012a).

We determined chance level EMG decoding performance by using phase-randomized versions of the ECoG signals to decode the EMGs (Bansal et al., 2011). We repeated this procedure 5000 times, and calculated the mean ± standard deviation of the resulting FVAF values to obtain an estimate of chance performance.

We also investigated the ability of ECoG to decode peak force, since that is an important aspect of daily living (e.g., picking up an object without crushing it). To this end, we tested whether (1) the accuracy of predicted peak force levels correlated with continuous force predictions, and (2) the variability in force peaks during a recording session was a factor in our ability to decode continuous force from ECoG. We defined peak force prediction accuracy as the median (for each subject) percent error between actual and predicted force, across the times of all peaks in actual force. Percent error was calculated as the difference in predicted and actual peak force, divided by the actual force. Peak force variability for each subject was estimated as the SD of peak forces generated during a recording session.

Results

Decoding continuous force using ECoG

We recorded from 10 subjects while they pinched a force sensor isometrically between thumb and index finger. Each subject performed 5–10 min of this behavior in the recording sessions presented here (Table 1). The hand used in the task was always contralateral to the recording array; this was the dominant hand for 4 subjects.

An example ECoG spectrogram during the task is shown in Fig. 1A, along with decoded and actual force produced by the subject (Fig. 1B). Power in the high gamma range (>70 Hz) increased at the onset of force application and is noticeably higher for higher force production. Lower frequencies (approximately 7 to 35 Hz, largely mu and beta bands, with some low gamma band) showed elevated power during rest, with suppression in power during active squeezing particularly evident around 20 Hz (beta band). This shows that beta suppression in ECoG is not exclusively linked to variation with kinematics, or even to movement, as this was an isometric task. Fig. 1B illustrates the close match between the decoded force (green trace) and the actual force (blue trace) during this time period. Supplemental Figs. SF2 through SF5 show additional examples from our data set.

We decoded grasp force with ECoG standard macroelectrodes in 7 subjects and medium-density macroelectrodes in 2 subjects. Subject S2 was undergoing a repeat resection and had too many subdural adhesions and therefore only received a microwire array. Using the Wiener cascade decoder, mean decoding accuracy across cross-validation folds ranged from 0.35 to 0.88 FVAF in the subjects with macroelectrodes (Fig. 2). Overall, the mean FVAF across those subjects (±SE) was 0.60 ± 0.06. (Decoding results using a simple linear filter are shown in Supplemental Information.) We also decoded force using signals from microwire arrays in 3 subjects, with intrasubject accuracy ranging from 0.22 to 0.52 (0.32 ± 0.10 mean ± SE overall). In one of two subjects who had both macroelectrodes and microwires implanted simultaneously (S3), force decoding was superior with microwires. In the other subject who had simultaneous implants (S4), macroelectrodes provided more accurate decoding (Fig. 2). The position of the microwire arrays was determined in part by the macro-grid location, and thus was not always located over the hand area of M1. We note that the two medium-density macro arrays (S8 and S10) provided highly accurate predictions, comparable with the best FVAF obtained using standard macroelectrodes (Fig. 2).

Due to clinical monitoring requirements and differences in recording preferences between institutions, the number of electrodes in each subject varied widely, ranging from 10 to 45, providing 60 to 270 possible features to serve as inputs to the decoder. For each patient, we selected the top 90% of features, ranked by their correlation to pinch force in the training data (see Table 1 for number of features used). Values for the regularization constant λ used in ridge regression were optimized for each session (see Methods) and ranged from 2 to 10.

Peak force levels ranged from 2 N to 69 N (see Table 1). Target-pursuit subjects applied slightly less peak force on average (21 ± 16 N; mean ± SD) compared to the self-paced subjects (peak force 28 ± 11 N, see Table 1). Across subjects, there was a strong correlation between error in peak force predictions and continuous FVAF ($R = -0.73$, $p = 0.02$, Spearman's correlation coefficient used due to the non-normality of the peak force predictions). There was no significant correlation between continuous force FVAF and peak force SD ($p = 0.22$, Spearman's correlation coefficient) for the subjects. The variability in peak force levels in the

Table 1
Details of the recordings in each subject. *S8 and S10 were implanted with medium-density ECoG arrays, rather than standard clinical microelectrode grids.

Subject	Hand dominance	Length of recording (min)	Number of squeezes	Mean ± SD peak force (N)	Macrocontacts	Macrofeatures selected	Microwires	Microwire features selected
S1	R	10	99	33 ± 10	16	86		
S2	R	5	41	35 ± 14			16	86
S3	L	5	15	29 ± 10	16	86	16	86
S4	R	5	60	10 ± 6	16	86	16	86
S5	R	10	463	29 ± 9	47	254		
S6	R	10	176	36 ± 7	45	243		
S7	L	10	57	39 ± 12	29	157		
S8	R	5	66	10 ± 1	63*	340		
S9	R	5	42	24 ± 5	10	54		
S10	R	10	196	19 ± 6	58*	313		

two different versions of the task (with and without visual feedback) was similar (see Supplemental Fig. SF1).

Decoding continuous EMG from ECoG

In subjects S2–S5, S7, S9, and S10, we recorded muscle activation from the flexor digitorum superficialis. ECoG decoding performance of these EMGs, measured using the FVAF, ranged from 0.23 to 0.82 using macroelectrode arrays (0.45 ± 0.09 mean ± SE, see Fig. 3). In 2 subjects, we decoded EMG with microwire data; performance was slightly lower (0.2 ± 0.07 mean ± SE), but still greater than chance (Fig. 3, dotted shaded line). It should be noted that not all subjects who completed the force task had EMG recordings. Comparing EMG decoding FVAF to force decoding FVAF for only those subjects in whom we recorded EMGs, we found no significant difference (*t*-test, $p = 0.52$). Not surprisingly, EMG prediction accuracy was highly correlated with force prediction accuracy ($R = 0.91$, $p = 0.01$). Supplemental Fig. SF5 shows example spectrographic and decoding data from our EMG data set.

Feature information

The LMP carried the most information about both force and EMG, followed by the 3 high gamma bands (Fig. 4). LMP decoding was significantly more accurate than decoding in any frequency band for both force (1-way ANOVA, $p < 10^{-5}$ for all LMP post-hoc tests) and EMG (1-way ANOVA, $p < 0.04$ for all LMP post-hoc tests). The 70–115 Hz band also provided more accurate decoding than either of the two low frequency bands for force ($p < 10^{-4}$), and more accuracy than the 7–20 Hz band for EMG ($p = 0.008$). In EMG but not force decoding, the 70–115 Hz band provided better decoding than the 200–300 Hz band ($p = 0.01$). We tested the influence of common average reference (CAR) filtering (McFarland et al., 1997) on single-band decoding, and found no significant changes in the decoding values for S1–S4 (S5–S10 were recorded with a hardware-based CAR).

Spatial localization of force representation

To find the anatomical focus of force decoding, we analyzed force-prediction performance using the LMP from individual electrodes. We achieved peak decoding accuracy for most subjects using signals from the primary motor cortex (Fig. 5). The highest force decoding accuracy was usually concentrated in 1 or 2 electrodes (e.g., subject S5 in Fig. 5). More distributed representations were also found, involving large areas of M1 (S6) or premotor cortex (S4). We found few sites of accurate decoding posterior to the central sulcus. For subject S8, who had a medium-density array, the most informative sites were concentrated in an area of approximately 50 mm^2. S10, also with a medium-density grid had a larger area of high-level decoding, covering most of the anterior half of the grid (Fig. 5).

In some subjects, we did find substantial force information in post-central areas (e.g., subject S1 in Fig. 5). This is not surprising, due to the continuous nature of the force task, with no defined trials or baseline periods. To determine the locus of force-related information across subjects, we grouped the macroelectrodes into three groups, based on anatomic region: M1, pre-central (including M1, pre-motor, and pre-frontal areas where applicable), and post-central. Supplemental Fig. SF6 shows

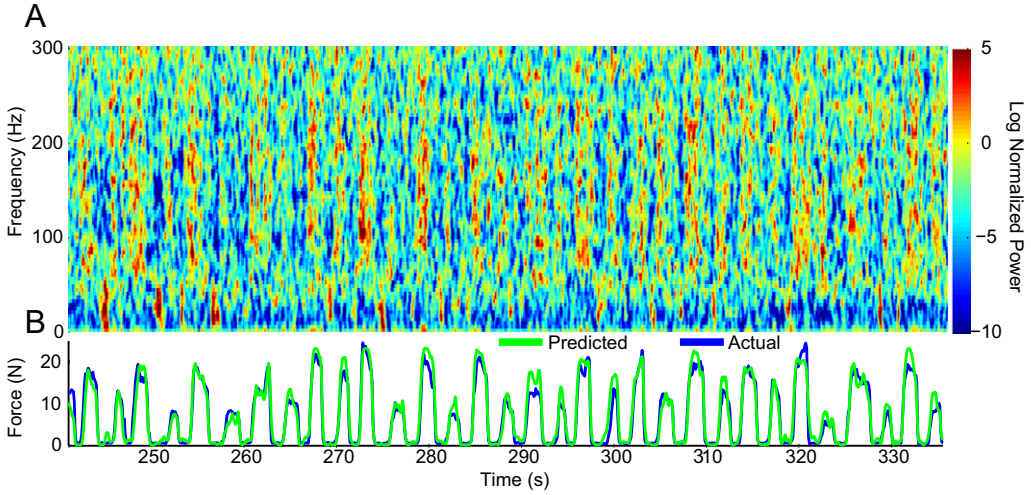

Fig. 1. ECoG modulation with grasp force for an exemplary subject. A, time-frequency spectrogram of log normalized power from subject S10. Individual pixels have been smoothed with a 3 × 3, 2D boxcar filter for display purposes. B, example of actual (blue) and predicted (green) force (using 90% of features; see Methods) from the same time segment of the recording. Overall, the mean (±SD) FVAF for force decoding in this recording session was 0.88 ± 0.04.

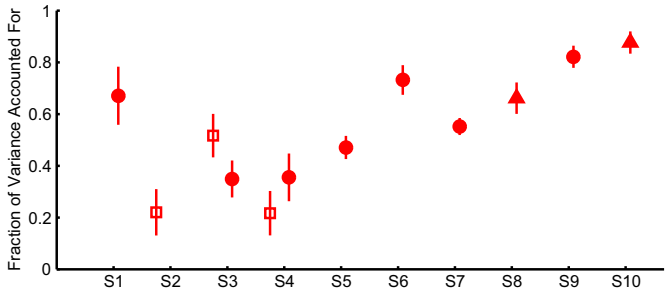

Fig. 2. Force decoding performance for all subjects. Mean FVAF (±SD) over the entire session for each subject is shown using macroelectrodes (filled circles) and microwires (open squares). The recordings for S8 and S10 were performed with medium-density macroelectrodes (filled triangle).

the designated regions for each subject. We implemented the decoding analysis independently for each region. In general, we observed that the pre-central region decoded force with an accuracy that was not significantly different from the accuracy when using all electrodes ($p = 0.15$, 1-way ANOVA with Tukey post-hoc, see Fig. SF7 in Supplemental Information). Post-central sites, on the other hand, were significantly worse at decoding force than M1, pre-central, or all electrodes ($p < 0.02$, Tukey post-hoc). This implies that our ensemble decoding was predominantly motor rather than sensory.

Three subjects (S8–S10) each completed an additional recording session, where they squeezed and released the force sensor while using their thumb and little finger, instead of their thumb and index finger. For these subjects, force decoding levels were slightly higher for little finger decoding (S8, 0.78 ± 0.10 mean ± SD; S9, 0.84 ± 0.05; S10, 0.84 ± 0.20) than they were for index finger decoding (S8, 0.66 ± 0.12; S9, 0.82 ± 0.09; S10, 0.79 ± 0.27; see Fig. 2). We applied our spatial analysis to the little finger data, and observed a shift inferiorly and anteriorly in the location of peak decoding accuracy (Fig. 6). The shift was particularly noticeable in S8 and S10, where the medium-density arrays showed the decoding focus to move from one electrode to a neighboring electrode (S8) or both move and spread out (S10). The shift was more difficult to precisely localize in subject S9, possibly due to the lower resolution of the electrode array.

Discussion

We sought to determine if grasp force and muscle activation levels could be decoded using cortical surface potentials. Our results demonstrated that ECoG could be used to decode continuous, variable isometric grasp force with high accuracy. We also found that ECoG contained a great deal of information about continuous finger muscle EMGs, similar to that about force. To our knowledge, this is the first study to demonstrate accurate decoding of continuous force using ECoG. Previously,

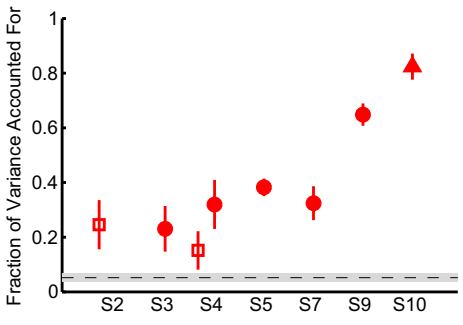

Fig. 3. Performance of finger flexor EMG decoding. Mean FVAF (±SD) for each subject is shown using macroelectrodes (filled circles), microwires (open squares), and medium-density macroelectrodes (filled triangle). Chance performance (dotted shaded line) was 0.05 ± 0.02 FVAF.

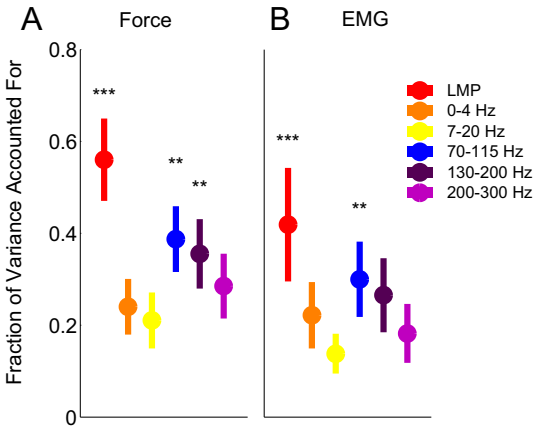

Fig. 4. Mean ± S.E. decoding performance across patients using single frequency bands for (A) force and (B) EMG with macroelectrodes. LMP performed significantly better than all other bands (***). The 70–115 Hz and 130–200 Hz bands performed better than the 0–4 Hz and 7–20 Hz bands (**). For EMG decoding, the 70–115 Hz band also performed significantly better than the 200–300 Hz band.

Pistohl et al. (2012) used a discrete classifier to identify 2 discrete levels of force with 70% accuracy during a reach-and-grasp task. Here, we show that accurate, continuous force decoding is possible using ECoG. While there was some variability among subjects, performance for some subjects was as high as force decoding using intracortical spikes in macaques (Carmena et al., 2003; Hendrix et al., 2009).

Information in ECoG features

The most information about force or EMG was contained in the LMP and the high gamma bands (70–115 Hz, 130–200 Hz, and 200–300 Hz; see Fig. 4). The high information in the LMP and the 70–115 Hz band is in agreement with prior studies of grasp decoding using ECoG (Pistohl et al., 2012). The LMP of ECoG contributed more, relative to the high gamma bands, than we have observed in our intracortical recordings during grasp. Also, the 70–115 Hz band had more information than the highest (200–300 Hz) gamma band, which contrasts with our findings using LFPs (Flint et al., 2012a).

We found evidence of mu and beta suppression around the onset of increasing force levels. However, features extracted from those frequencies provided poor decoding of continuous force. This supports previous findings that low frequency oscillations can be used to differentiate movement from rest, but are not highly modulated with the details of movement (Chestek et al., 2013; Flint et al., 2012b; Murthy and Fetz, 1996).

It is unlikely that these results could be explained by movement artifacts of the limbs or eyes. In these experiments, we measured isometric force, which does not require accompanying hand or arm movements. Subjects were explicitly instructed not to move, and we monitored them to ensure that they remained motionless. Any movement artifact that might influence the ECoG signals would have been small in amplitude (because of the lack of overt hand/arm movements) and low in frequency. Since 7 of the subjects had no visual force feedback, it would be very unlikely that eye movements would track force well in those subjects.

Force representation in the cortex

In general, there was substantial variation in decoding accuracy among our subjects. This was likely due to differences in coverage of their motor cortices, which was dictated by clinical considerations. However, it is also possible that force-encoding regions of cortex are spread diffusely throughout motor areas, as has been hypothesized for cortical representation of individual finger movements (Schieber and

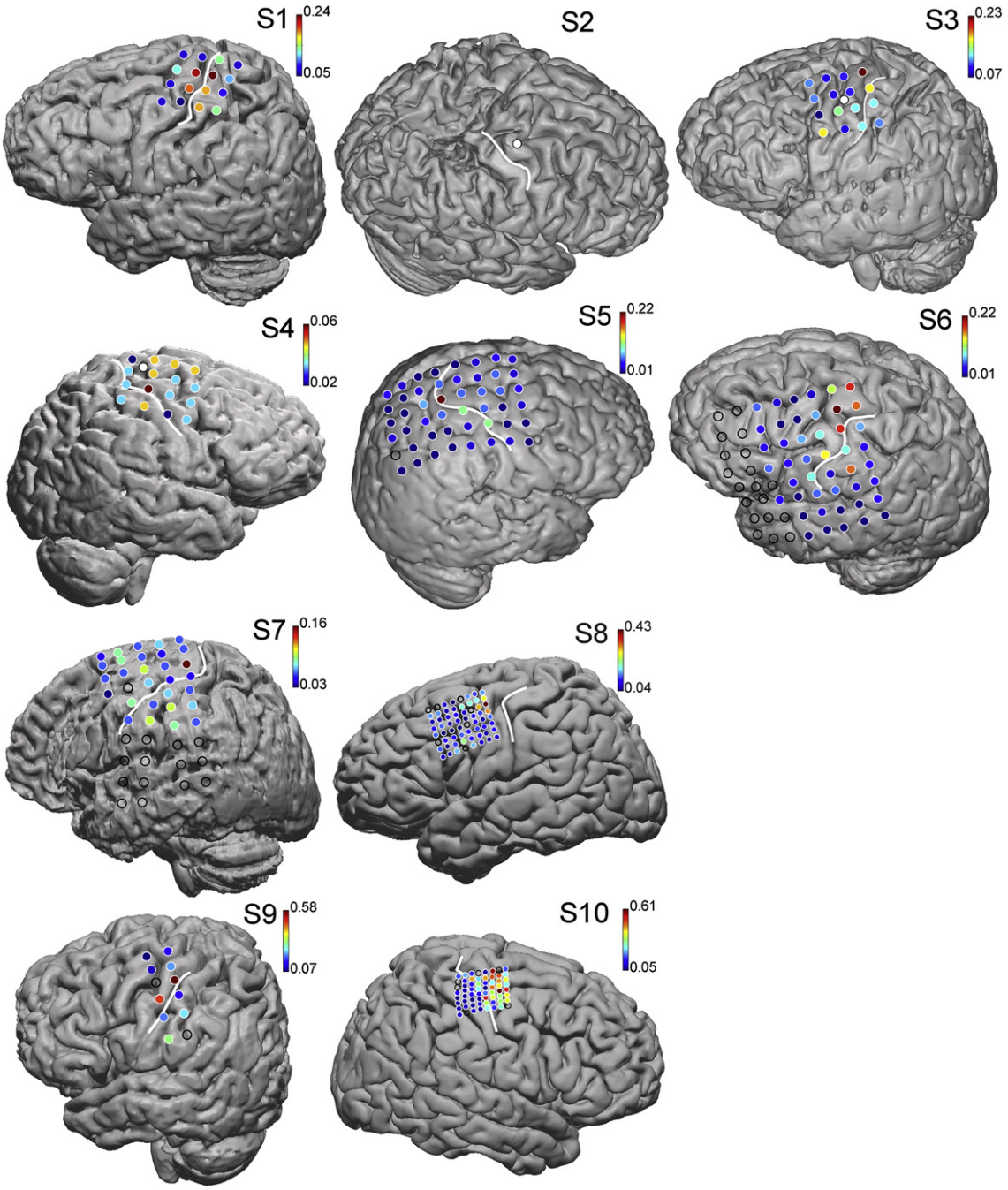

Fig. 5. Single electrode force decoding performance using the LMP in each subject. White circles with black boundaries in S2, S3, and S4 mark the positions of microwire arrays. Central sulcus in each patient is marked with a white line. The color of each macroelectrode location indicates the FVAF for that electrode. The range of colors is scaled for each subject such that dark red indicates the best-performing electrode, and dark blue indicates the worst-performing electrode. For subjects S5–S10, some channels were excluded from the analysis (empty circles) due to high-amplitude noise. Subject S7 had some left frontal lobe atrophy from an intrauterine stroke. The electrodes for S8 and S10 are superimposed on a standard brain, since these subjects could not have MRIs.

Poliakov, 1998). Such a distributed arrangement is one possible explanation for the finding that only a fraction of M1 and PMd neurons modulate their firing rates with grasp force (Hendrix et al., 2009). An alternative hypothesis is that traditional macroelectrode grids may simply be missing the precise cortical regions most informative about pinch force because their spatial resolution is too low. Our decoding of index finger vs. little finger flexion (Fig. 6) provides some evidence in support of this hypothesis. Using medium-density ECoG grids, we observed a shift of 4 mm in the location of peak decoding accuracy in S8. In S10, the peak decoding location shifted by approximately the same amount, though it also spread out in space. We also observed this spreading of activation in S9, though the coarse spatial sampling of the standard grid made it difficult to be certain whether the peak decoding location had shifted or not. A diffuse representation when applying force with different fingers is consistent with findings from studies using ECoG to decoding finger kinematics (Kubanek et al., 2009). It is also possible that more widespread activation during little finger squeezes may have been due to weaker muscles than in the index finger or to coupling between the fingers, leading the subjects to squeeze partially with additional fingers besides just thumb and little finger.

Previous work has shown an optimal spacing for recording subdural signals, to avoid spatial aliasing, is approximately 2 mm for the human cortex (Slutzky et al., 2010). Higher spatial resolution than is possible with standard macroelectrode grids would likely benefit ECoG studies,

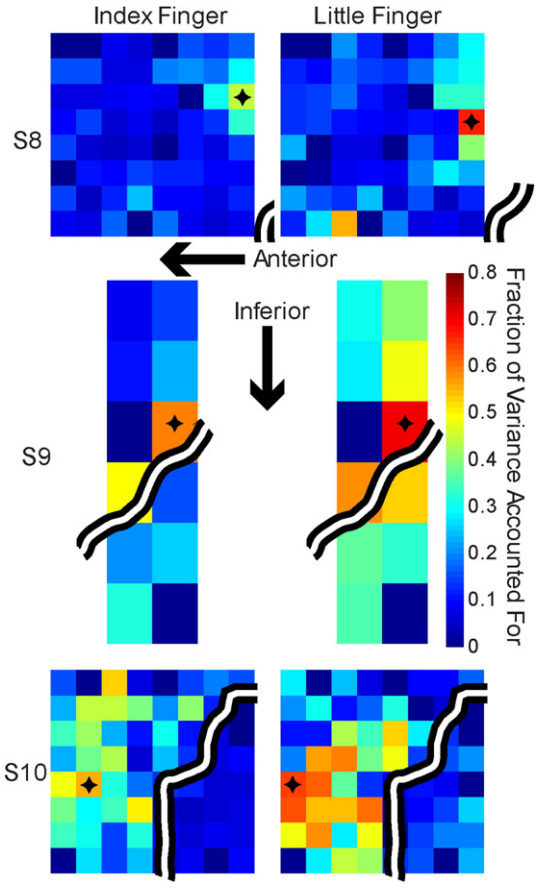

Fig. 6. Single electrode force decoding performance using index vs. little fingers in subjects S8–S10. The display for S10 has been flipped horizontally because S10 was a right-hemisphere implant. Central sulcus is shown using a white-on-black line. The most informative electrode with LMP (✦) shifted by approximately 4 mm inferior in subject S8, and 4 mm anterior in S10. In S9, we did not detect a change in the peak decoding site. In all three subjects, there was a spreading of activation in the anterior and inferior directions with little finger force as compared to index finger force.

whether investigating basic facts about the motor system or developing applications such as BMIs.

We observed the most information about force in signals recorded from the primary motor cortex. We did find substantial force-related information in other pre-central areas besides M1, particularly in subject S1 (Fig. 5). There were few sites of accurate decoding posterior to the central sulcus, though again spatial sampling was limited by clinical necessity. We note that signals from S5 to S10 were common average referenced prior to digitization. Although it is true that CAR can sometimes introduce artifacts in a few electrodes when there is signal in most of the other electrodes (Desmedt et al., 1990), we saw no difference in decoding with or without the CAR in S1–S4. Thus, we would not expect CAR to adversely impact our ability to draw conclusions from the data based on electrode location.

EMG decoding with ECoG

EMG signals contain spectral power at higher frequencies than kinematics (Flint et al., 2012a). Despite this fact, EMG has been decoded as accurately as kinematics using intracortical spikes or LFPs (Flint et al., 2012a, 2012b). In the current study, ECoG signals provided similar performance decoding EMG compared with decoding force, when considering only those subjects in whom EMGs were recorded. It should be noted that the contribution of high-gamma ECoG power to both force and EMG (Fig. 4) was lower than we have observed in our intracortical LFP studies. The lower information in the high gamma range may be an indication that surface potentials, in general, retain less high frequency power than field potentials recorded from penetrating microelectrodes, as suggested by performance observed by Markowitz et al. (2011). A study using medium-density ECoG grids in monkeys demonstrated slightly higher decoding of intramuscular EMG, though on a very limited data set (Shin et al., 2012). Thus, it remains to be seen whether ECoG can provide enough information about EMG to control FES.

Implications for BMIs

The results presented here suggest that ECoG could be used to accurately control grasp force. Such regulation will be a critical design feature of any effective hand neuroprosthesis, whether robotic or FES-driven. Decoding grasp force directly, rather than using a surrogate such as finger position or velocity, would be a more intuitive method of control, especially for sustained grasp. Given the high variability of decoding performance with different placement of electrodes in this and other studies (Acharya et al., 2010; Schalk et al., 2007), precise localization of electrodes is critical to achieving high-performance control of grasp force. We conclude that medium- or high-density electrodes, if optimally located, might give more detailed information about grasping force than standard clinical arrays. This seems particularly important when decoding higher-dimensional movements or many EMGs, as opposed to the single DOF in this study.

Other groups have successfully demonstrated that a few paralyzed patients can control BMIs using intracortical spiking activity (Collinger et al., 2013; Hochberg et al., 2012). Despite these groundbreaking studies, it is still not clear for how long currently-available recording technologies will be able to successfully record high numbers of spikes (Simeral et al., 2011). The longevity of acquired signals is a particularly relevant issue for people with paralysis, for whom an implanted device should ultimately function for several decades to avoid requiring multiple surgeries for re-implantation. Field potentials provide information about movement even when spikes are absent (Flint et al., 2012b), and may provide a longer-lasting signal source than spikes (Andersen et al., 2004). In monkeys, ECoG signals are stable for 4–5 months in offline decoding (Chao et al., 2010), and intracortical LFPs are highly stable for a year in a closed-loop BMI (Flint et al., 2013). Subdural signals are intermediate in invasiveness, signal bandwidth and spatial resolution (Slutzky et al., 2010) between intracortical and noninvasive signals like the electroencephalogram. Further, implanted subdural electrodes have shown stable impedances for over a year in humans (Sillay et al., 2013). Thus, ECoG may provide an optimal control signal for BMIs, depending on the application.

Epidural signals should provide similar signal quality to subdural signals (Slutzky et al., 2010) with less risk of encephalitis or subdural hemorrhage since the dura is not incised. As such, they could provide an even safer alternative to ECoG while still allowing accurate control of movement (Rouse et al., 2013; Shimoda et al., 2012; Slutzky et al., 2011). Together, these intermediate signal sources could provide clinicians with an important signal source for BMI applications.

Supplementary data to this article can be found online at http://dx.doi.org/10.1016/j.neuroimage.2014.07.049.

Acknowledgments

We thank Eric Lindberg, Carolina Carmona, Jun Yao, and Michael Scheid for their assistance in collecting data, and Jules Dewald for providing the force transducer. We also thank Micheal Macken and Elizabeth Gerard for assisting subject recruitment at Northwestern. Finally, we greatly appreciate the assistance of our technicians and of course our subjects for participating in this study. This study was supported by the Brain Research Foundation (BRF SG 2009-14), the Northwestern Memorial Foundation Dixon Translational Research Grant Program (supported in part by NIH grant UL1 RR025741 from the National Center for Research Resources), the Paralyzed Veterans of America

(grant #2728), the Doris Duke Charitable Foundation Clinical Scientist Development Award (grant #2011039), the NSF award 1134575, and an American Brain Foundation grant to AHD.

Conflict of interest

The authors have no conflict of interest to disclose.

References

Acharya, S., Fifer, M.S., Benz, H.L., Crone, N.E., Thakor, N.V., 2010. Electrocorticographic amplitude predicts finger positions during slow grasping motions of the hand. J. Neural Eng. 7, 046002.

Aggarwal, V., Acharya, S., Tenore, F., Shin, H.C., Etienne-Cummings, R., Schieber, M.H., Thakor, N.V., 2008. Asynchronous decoding of dexterous finger movements using M1 neurons. IEEE Trans. Neural Syst. Rehabil. Eng. 16, 3–14.

Aggarwal, V., Mollazadeh, M., Davidson, A.G., Schieber, M.H., Thakor, N.V., 2013. State-based decoding of hand and finger kinematics using neuronal ensemble and LFP activity during dexterous reach-to-grasp movements. J. Neurophysiol. 109, 3067–3081.

Andersen, R.A., Musallam, S., Pesaran, B., 2004. Selecting the signals for a brain–machine interface. Curr. Opin. Neurobiol. 14, 720–726.

Bansal, A.K., Vargas-Irwin, C.E., Truccolo, W., Donoghue, J.P., 2011. Relationships among low-frequency local field potentials, spiking activity, and three-dimensional reach and grasp kinematics in primary motor and ventral premotor cortices. J. Neurophysiol. 105, 1603–1619.

Ben Hamed, S., Schieber, M.H., Pouget, A., 2007. Decoding M1 neurons during multiple finger movements. J. Neurophysiol. 98, 327–333.

Boudreau, M.J., Brochier, T., Pare, M., Smith, A.M., 2001. Activity in ventral and dorsal premotor cortex in response to predictable force-pulse perturbations in a precision grip task. J. Neurophysiol. 86, 1067–1078.

Carmena, J.M., Lebedev, M.A., Crist, R.E., O'Doherty, J.E., Santucci, D.M., Dimitrov, D.F., Patil, P. G., Henriquez, C.S., Nicolelis, M.A., 2003. Learning to control a brain–machine interface for reaching and grasping by primates. PLoS Biol. 1, 1–16.

Castiello, U., Begliomini, C., 2008. The cortical control of visually guided grasping. Neuroscientist 14, 157–170.

Chao, Z.C., Nagasaka, Y., Fujii, N., 2010. Long-term asynchronous decoding of arm motion using electrocorticographic signals in monkeys. Front. Neuroenerg. 3, 1–10.

Chestek, C.A., Gilja, V., Blabe, C.H., Foster, B.L., Shenoy, K.V., Parvizi, J., Henderson, J.M., 2013. Hand posture classification using electrocorticography signals in the gamma band over human sensorimotor brain areas. J. Neural Eng. 10, 026002.

Collinger, J.L., Wodlinger, B., Downey, J.E., Wang, W., Tyler-Kabara, E.C., Weber, D.J., McMorland, A.J., Velliste, M., Boninger, M.L., Schwartz, A.B., 2013. High-performance neuroprosthetic control by an individual with tetraplegia. Lancet 381, 557–564.

Danion, F., Diamond, J.S., Flanagan, J.R., 2013. Separate contributions of kinematic and kinetic errors to trajectory and grip force adaptation when transporting novel hand-held loads. J. Neurosci. 33, 2229–2236.

Davare, M., Kraskov, A., Rothwell, J.C., Lemon, R.N., 2011. Interactions between areas of the cortical grasping network. Curr. Opin. Neurobiol. 21, 565–570.

Desmedt, J.E., Chalklin, V., Tomberg, C., 1990. Emulation of somatosensory evoked potential (SEP) components with the 3-shell head model and the problem of 'ghost potential fields' when using an average reference in brain mapping. Electroencephalogr. Clin. Neurophysiol. 77, 243–258.

Ethier, C., Oby, E.R., Bauman, M.J., Miller, L.E., 2012. Restoration of grasp following paralysis through brain-controlled stimulation of muscles. Nature 485, 368–371.

Evarts, E.V., Fromm, C., Kroller, J., Jennings, V.A., 1983. Motor cortex control of finely graded forces. J. Neurophysiol. 49, 1199–1215.

Fagg, A.H., Ojakangas, G.W., Miller, L.E., Hatsopoulos, N.G., 2009. Kinetic trajectory decoding using motor cortical ensembles. IEEE Trans. Neural Syst. Rehabil. Eng. 17, 487–496.

Fifer, M., Hotson, G., Wester, B., McMullen, D., Wang, Y., Johannes, M., Katyal, K., Helder, J., Para, M., Vogelstein, R.J., Anderson, W., Thakor, N., Crone, N., 2014. Simultaneous neural control of simple reaching and grasping with the modular prosthetic limb using intracranial EEG. IEEE Trans. Neural Syst. Rehabil. Eng. 22 (3), 695–705.

Flint, R.D., Ethier, C., Oby, E.R., Miller, L.E., Slutzky, M.W., 2012a. Local field potentials allow accurate decoding of muscle activity. J. Neurophysiol. 108, 18–24.

Flint, R.D., Lindberg, E.W., Jordan, L.R., Miller, L.E., Slutzky, M.W., 2012b. Accurate decoding of reaching movements from field potentials in the absence of spikes. J. Neural Eng. 9, 046006.

Flint, R.D., Wright, Z.A., Scheid, M.R., Slutzky, M.W., 2013. Long term, stable brain machine interface performance using local field potentials and multiunit spikes. J. Neural Eng. 10, 056005.

Hendrix, C.M., Mason, C.R., Ebner, T.J., 2009. Signaling of grasp dimension and grasp force in dorsal premotor cortex and primary motor cortex neurons during reach to grasp in the monkey. J. Neurophysiol. 102, 132–145.

Hepp-Reymond, M., Kirkpatrick-Tanner, M., Gabernet, L., Qi, H.X., Weber, B., 1999. Context-dependent force coding in motor and premotor cortical areas. Exp. Brain Res. 128, 123–133.

Hermes, D., Miller, K.J., Noordmans, H.J., Vansteensel, M.J., Ramsey, N.F., 2010. Automated electrocorticographic electrode localization on individually rendered brain surfaces. J. Neurosci. Methods 185, 293–298.

Hochberg, L.R., Serruya, M.D., Friehs, G.M., Mukand, J.A., Saleh, M., Caplan, A.H., Branner, A., Chen, D., Penn, R.D., Donoghue, J.P., 2006. Neuronal ensemble control of prosthetic devices by a human with tetraplegia. Nature 442, 164–171.

Hochberg, L.R., Bacher, D., Jarosiewicz, B., Masse, N.Y., Simeral, J.D., Vogel, J., Haddadin, S., Liu, J., Cash, S.S., van der Smagt, P., Donoghue, J.P., 2012. Reach and grasp by people with tetraplegia using a neurally controlled robotic arm. Nature 485, 372–375.

Hunter, I.W., Korenberg, M.J., 1986. The identification of nonlinear biological systems: Wiener and Hammerstein cascade models. Biol. Cybern. 55, 135–144.

Krakauer, J.W., Ghilardi, M.F., Ghez, C., 1999. Independent learning of internal models for kinematic and dynamic control of reaching. Nat. Neurosci. 2, 1026–1031.

Kubanek, J., Miller, K.J., Ojemann, J.G., Wolpaw, J.R., Schalk, G., 2009. Decoding flexion of individual fingers using electrocorticographic signals in humans. J. Neural Eng. 6, 066001.

Markowitz, D.A., Wong, Y.T., Gray, C.M., Pesaran, B., 2011. Optimizing the decoding of movement goals from local field potentials in macaque cortex. J. Neurosci. 31, 18412–18422.

McFarland, D.J., McCane, L.M., David, S.V., Wolpaw, J.R., 1997. Spatial filter selection for EEG-based communication. Electroencephalogr. Clin. Neurophysiol. 103, 386–394.

Mehring, C., Nawrot, M.P., de Oliveira, S.C., Vaadia, E., Schulze-Bonhage, A., Aertsen, A., Ball, T., 2004. Comparing information about arm movement direction in single channels of local and epicortical field potentials from monkey and human motor cortex. J. Physiol. Paris 98, 498–506.

Miller, K.J., Makeig, S., Hebb, A.O., Rao, R.P., denNijs, M., Ojemann, J.G., 2007. Cortical electrode localization from X-rays and simple mapping for electrocorticographic research: the "Location on Cortex" (LOC) package for MATLAB. J. Neurosci. Methods 162, 303–308.

Miller, K.J., Zanos, S., Fetz, E.E., den Nijs, M., Ojemann, J.G., 2009. Decoupling the cortical power spectrum reveals real-time representation of individual finger movements in humans. J. Neurosci. 29, 3132–3137.

Moritz, C.T., Perlmutter, S.I., Fetz, E.E., 2008. Direct control of paralysed muscles by cortical neurons. Nature 456, 639–642.

Murthy, V.N., Fetz, E.E., 1996. Oscillatory activity in sensorimotor cortex of awake monkeys: synchronization of local field potentials and relation to behavior. J. Neurophysiol. 76, 3949–3967.

Pistohl, T., Schulze-Bonhage, A., Aertsen, A., Mehring, C., Ball, T., 2012. Decoding natural grasp types from human ECoG. Neuroimage 59, 248–260.

Pohlmeyer, E.A., Oby, E.R., Perreault, E.J., Solla, S.A., Kilgore, K.L., Kirsch, R.F., Miller, L.E., 2009. Toward the restoration of hand use to a paralyzed monkey: brain-controlled functional electrical stimulation of forearm muscles. PLoS One 4, e5924.

Rouse, A.G., Williams, J.J., Wheeler, J.J., Moran, D.W., 2013. Cortical adaptation to a chronic micro-electrocorticographic brain computer interface. J. Neurosci. 33, 1326–1330.

Schalk, G., McFarland, D.J., Hinterberger, T., Birbaumer, N., Wolpaw, J.R., 2004. BCI2000: a general-purpose brain-computer interface (BCI) system. IEEE Trans. Biomed. Eng. 51, 1034–1043.

Schalk, G., Kubanek, J., Miller, K.J., Anderson, N.R., Leuthardt, E.C., Ojemann, J.G., Limbrick, D., Moran, D., Gerhardt, L.A., Wolpaw, J.R., 2007. Decoding two-dimensional movement trajectories using electrocorticographic signals in humans. J. Neural Eng. 4, 264–275.

Schieber, M.H., Poliakov, A.V., 1998. Partial inactivation of the primary motor cortex hand area: effects on individuated finger movements. J. Neurosci. 18, 9038–9054.

Shimoda, K., Nagasaka, Y., Chao, Z.C., Fujii, N., 2012. Decoding continuous three-dimensional hand trajectories from epidural electrocorticographic signals in Japanese macaques. J. Neural Eng. 9, 036015.

Shin, D., Watanabe, H., Kambara, H., Nambu, A., Isa, T., Nishimura, Y., Koike, Y., 2012. Prediction of muscle activities from electrocorticograms in primary motor cortex of primates. PLoS One 7, e47992.

Sillay, K.A., Rutecki, P., Cicora, K., Worrell, G., Drazkowski, J., Shih, J.J., Sharan, A.D., Morrell, M. J., Williams, J., Wingeier, B., 2013. Long-term measurement of impedance in chronically implanted depth and subdural electrodes during responsive neurostimulation in humans. Brain Stimul. 6, 718–726.

Simeral, J.D., Kim, S.P., Black, M.J., Donoghue, J.P., Hochberg, L.R., 2011. Neural control of cursor trajectory and click by a human with tetraplegia 1000 days after implant of an intracortical microelectrode array. J. Neural Eng. 8, 025027.

Slutzky, M.W., Jordan, L.R., Krieg, T., Chen, M., Mogul, D.J., Miller, L.E., 2010. Optimal spacing of surface electrode arrays for brain–machine interface applications. J. Neural Eng. 7, 26004.

Slutzky, M.W., Jordan, L.R., Lindberg, E.W., Lindsay, K.E., Miller, L.E., 2011. Decoding the rat forelimb movement direction from epidural and intracortical field potentials. J. Neural Eng. 8, 036013.

Spinks, R.L., Kraskov, A., Brochier, T., Umilta, M.A., Lemon, R.N., 2008. Selectivity for grasp in local field potential and single neuron activity recorded simultaneously from M1 and F5 in the awake macaque monkey. J. Neurosci. 28, 10961–10971.

Suminski, A.J., Tkach, D.C., Fagg, A.H., Hatsopoulos, N.G., 2010. Incorporating feedback from multiple sensory modalities enhances brain–machine interface control. J. Neurosci. 30, 16777–16787.

Townsend, B.R., Subasi, E., Scherberger, H., 2011. Grasp movement decoding from premotor and parietal cortex. J. Neurosci. 31, 14386–14398.

Vargas-Irwin, C.E., Shakhnarovich, G., Yadollahpour, P., Mislow, J.M., Black, M.J., Donoghue, J.P., 2010. Decoding complete reach and grasp actions from local primary motor cortex populations. J. Neurosci. 30, 9659–9669.

Wang, W., Collinger, J.L., Degenhart, A.D., Tyler-Kabara, E.C., Schwartz, A.B., Moran, D.W., Weber, D.J., Wodlinger, B., Vinjamuri, R.K., Ashmore, R.C., Kelly, J.W., Boninger, M.L., 2013. An electrocorticographic brain interface in an individual with tetraplegia. PLoS One 8, e55344.

Wang, P.T., King, C.E., Shaw, S.J., Millett, D.E., Liu, C.Y., Chui, L.A., Nenadic, Z., Do, A.H., 2013. A co-registration approach for electrocorticogram electrode localization using post-implantation MRI and CT of the head. IEEE EMBS Conf on Neural Eng.

Westwick, D.T., Pohlmeyer, E.A., Solla, S.A., Miller, L.E., Perreault, E.J., 2006. Identification of multiple-input systems with highly coupled inputs: application to EMG prediction from multiple intracortical electrodes. Neural Comput. 18, 329–355.

Yanagisawa, T., Hirata, M., Saitoh, Y., Goto, T., Kishima, H., Fukuma, R., Yokoi, H., Kamitani, Y., Yoshimine, T., 2011. Real-time control of a prosthetic hand using human electrocorticography signals. J. Neurosurg. 114, 1715–1722.

Zhuang, J., Truccolo, W., Vargas-Irwin, C., Donoghue, J.P., 2010. Reconstructing grasping motions from high-frequency local field potentials in primary motor cortex. Conference Proceedings: Annual International Conference of the IEEE Engineering in Medicine and Biology Society IEEE Engineering in Medicine and Biology Society Conference, pp. 4347–4350.